Biophysical Journal, Volume *113*

Supplemental Information

A Hinged Signal Peptide Hairpin Enables Tat-Dependent Protein Translocation

Shruthi Hamsanathan, Tamil S. Anthonymuthu, Umesh K. Bageshwar, and Siegfried M. Musser

Table S1: Primers Used to Generate Mutants

Plasmid/Mutant	Forward Primer (5' -> 3')	Reverse Primer (5' -> 3')
pSufI - S2C	ATA CAT ATG TGT CTC AGT CGG	ATC TCC TTC TTA AAG TTA AAC AA
pSufI - F8C	GGC GTC AGT GTA TTC AGG C	GAC TGA GTG ACA TAT GTA TAT
pSufI - I9C	CGG CGT CAG TTC TGT CAG GCA TCG GGG	ACT GAG TGA CAT ATG TAT ATC TCC TTC
pSufI - Q10C	ATT GCA CTT ATT GCA GGC GCT	CCC CGA TGC ACA AAT GAA CTG
pSufI - A11C	GCA CTT ATT GCA GGC GCT GTT	AAT CCC CGA ACA CTG AAT GAA
pSufI - S12C	TTC ATT CAG GCA TGT GGG ATT GCA CTT	CTG ACG CCG ACT GAG TGA CAT ATG TAT
pSufI - G13C	CAG GCA TCG TGT ATT GCA CTT	AAT GAA CTG ACG CCG ACT GAG
pSufI - I14C	TGC AGG CGC TGT TCC CCT G	ATA AGT GCA CAC CCC GAT G
pSufI - A15C	TCG GGG ATT TGT CTT ATT GCA	TGC CTG AAT GAA CTG ACG CCG
pSufI - L16C	GGG ATT GCA TGT ATT GCA GGC	CGA TGC CTG AAT GAA CTG ACG
pSufI - A18C	GCA CTT ATT TGT GGC GCT GTT	AAT CCC CGA TGC CTG AAT GAA
pSufI - G19C	CTT ATT GCA TGT GCT GTT CCC	TGC AAT CCC CGA TGC CTG AAT
pSufI - A20C	CTT ATT GCA GGC TGT GTT CCC CTG AAG	TGC AAT CCC CGA TGC CTG AAT GAA CTG
pSufI - V21C	GCA GGC GCT TGT CCC CTG AAG	AAT AAG TGC AAT CCC CGA TGC C
pSufI - L23C	GCT GTT CCC TGT AAG GCC AGC	GCC TGC AAT AAG TGC AAT CCC C
pSufI - A25C	CCC CTG AAG TGT AGC GCA GCC	AAC AGC GCC TGC AAT AAG TGC AA
pSufI - A27C	CAA CCG CTA CAG CAA CCG CTA CCC GTT	CTG TTG CCC GGC ACA GCT GGC CTT CAG
pSufI - Q30C	GCA GCC GGG TGT CAG CAA CCG CTA	TAG CGG TTG CTG ACA CCC GGC TGC
pSufI - P33C	GCC GGG CAA CAG CAA TGT CTA CCC GTT CCG	CGG AAC GGG TAG ACA TTG CTG TTG CCC GGC
pSufI - V36C	AGC AAC CGC TAC CCT GTC CGC CGC TGC TTG	CAA GCA GCG GCG GAC AGG GTA GCG GTT GCT
pSufI - R44C	TGC TTG AAT CTC GCT GTG GGC AAC CGC TG	CAG CGG TTG CCC ACA GCG AGA TTC AAG CA
pSufI - F49C	GGG CAA CCG CTG TGT ATG ACT GTA CAA CG	CGT TGT ACA GTC ATA CAC AGC GGT TGC CC
pSufI - M338C	AGT CTT CCG TGT CGC TTG CTG	GTC TGT GAC CAG CGG CAG AAG
pSufI - W441C	GAA GTG CGC ACA GGA AGG CTG	CCG TTC TAC TTC AAC AGT CAG AC
pSufI - Q31C	CCC GTT CCG CCG CTG CTT GA	TAG CGG TTG ACA TTG CCC GGC
pSufI - Y221C	CAA AGC CCG TGT GTT GAA GTC	TAC ACC GTT AAC CAG CAG CGT
pSufI - 12C/25C	CCC CTG AAG TGT AGC GCA GCC	AAC AGC GCC TGC AAT AAG TGC AA
pTatAC	ATG TCT GTA GAA GAT ACT	GTT TAC ACC TGC TCT TTA
pTatBC	ATG TTT GAT ATC GGT TTT	TAT ACG TTA CAC GGC CAT
pTatC	ATG TCT GTA GAA GAT ACT	TAT ACG TTA CAC GGC CAT
pSufI KK	ACT CAG TAA GAA ACA GTT CAT TC	GAC ATA TGT ATA TCT CCT TCT TA

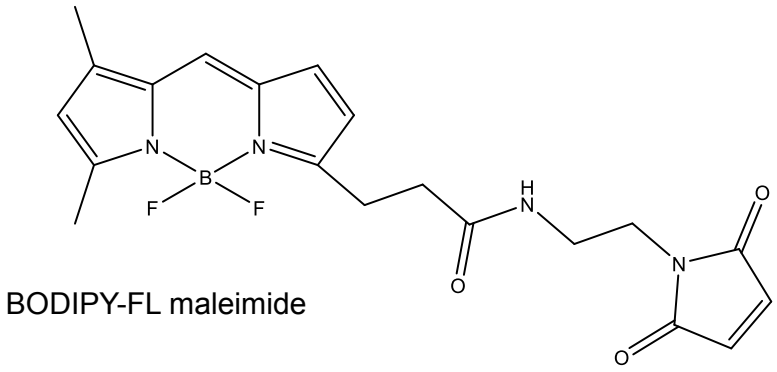

BODIPY-FL maleimide

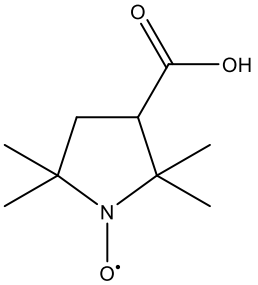

3-Carboxy-PROXYL
(3-CP)

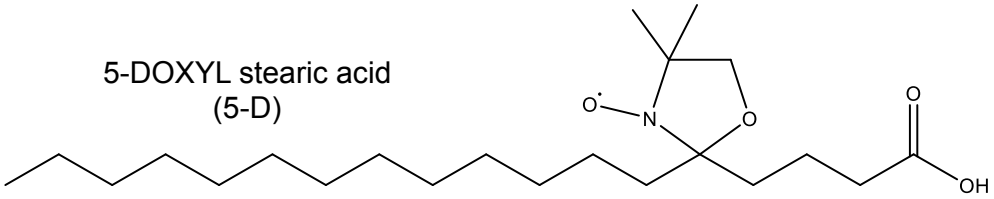

5-DOXYL stearic acid
(5-D)

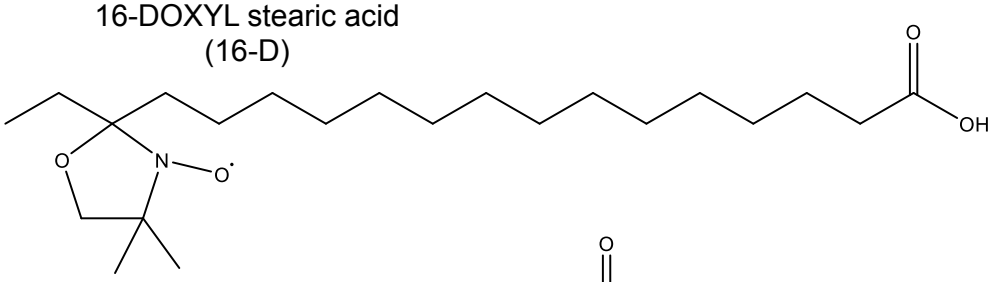

16-DOXYL stearic acid
(16-D)

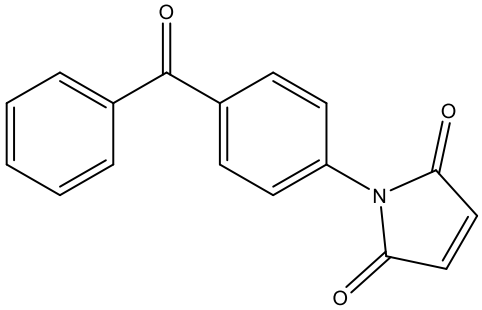

4-(maleimido)benzophenone

Figure S1. Structures of the BODIPY-FL Cysteine-reactive Fluorescent Probe, the Nitroxide Quenchers, and the Photocrosslinker used in this Study.

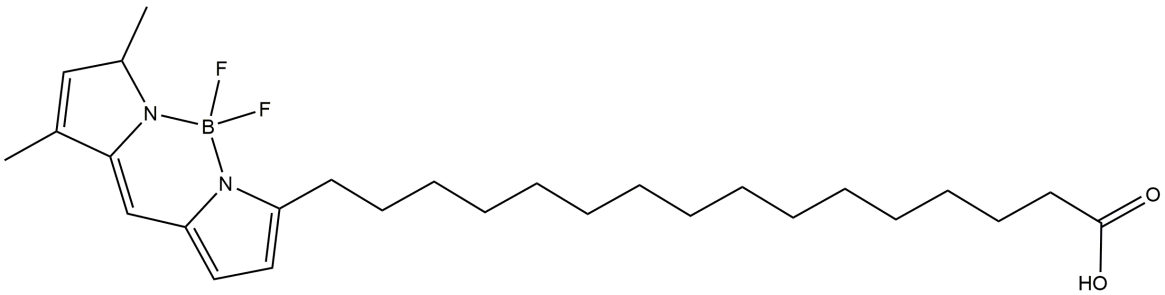

BODIPY-FL C_{16} Palmitic Acid

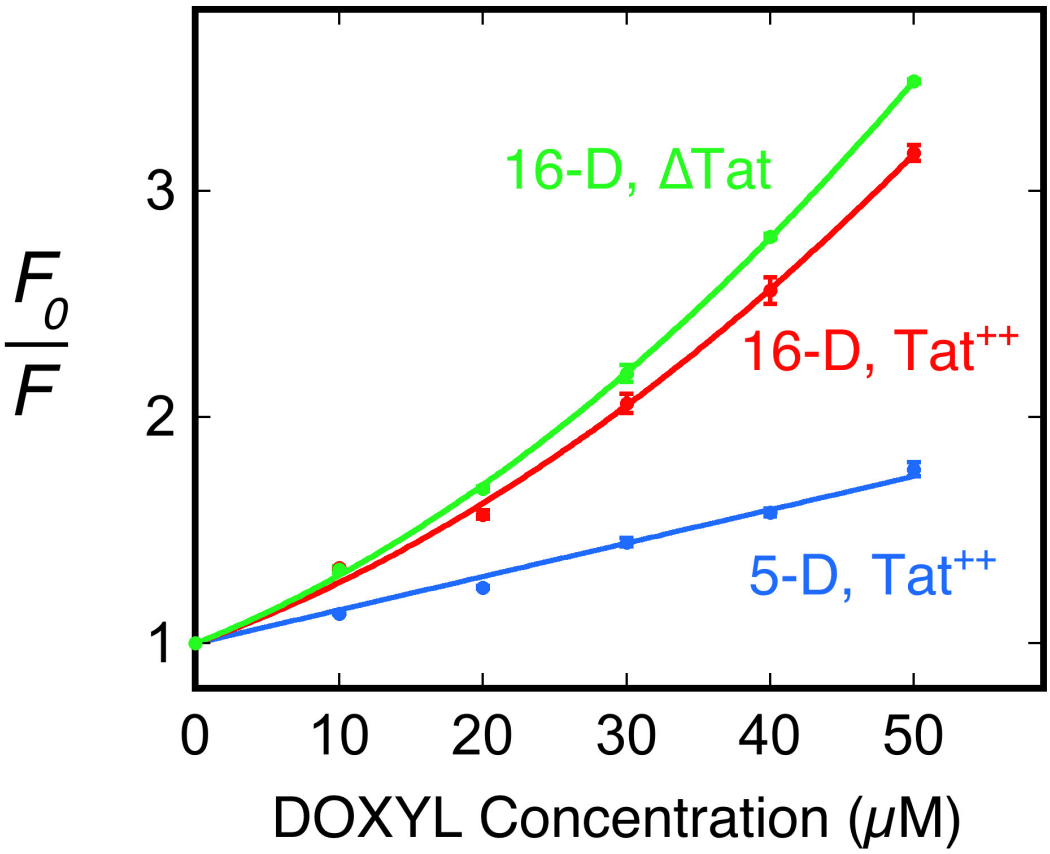

Figure S2. Stern-Volmer Quenching of BODIPY-FL at the C_{16} Position of Palmitic Acid Incorporated into ΔTat and Tat^{++} IMVs. Quenching was performed as in Figure 2. The data were fit to a first (5-D) or second (16-D) degree polynomial.

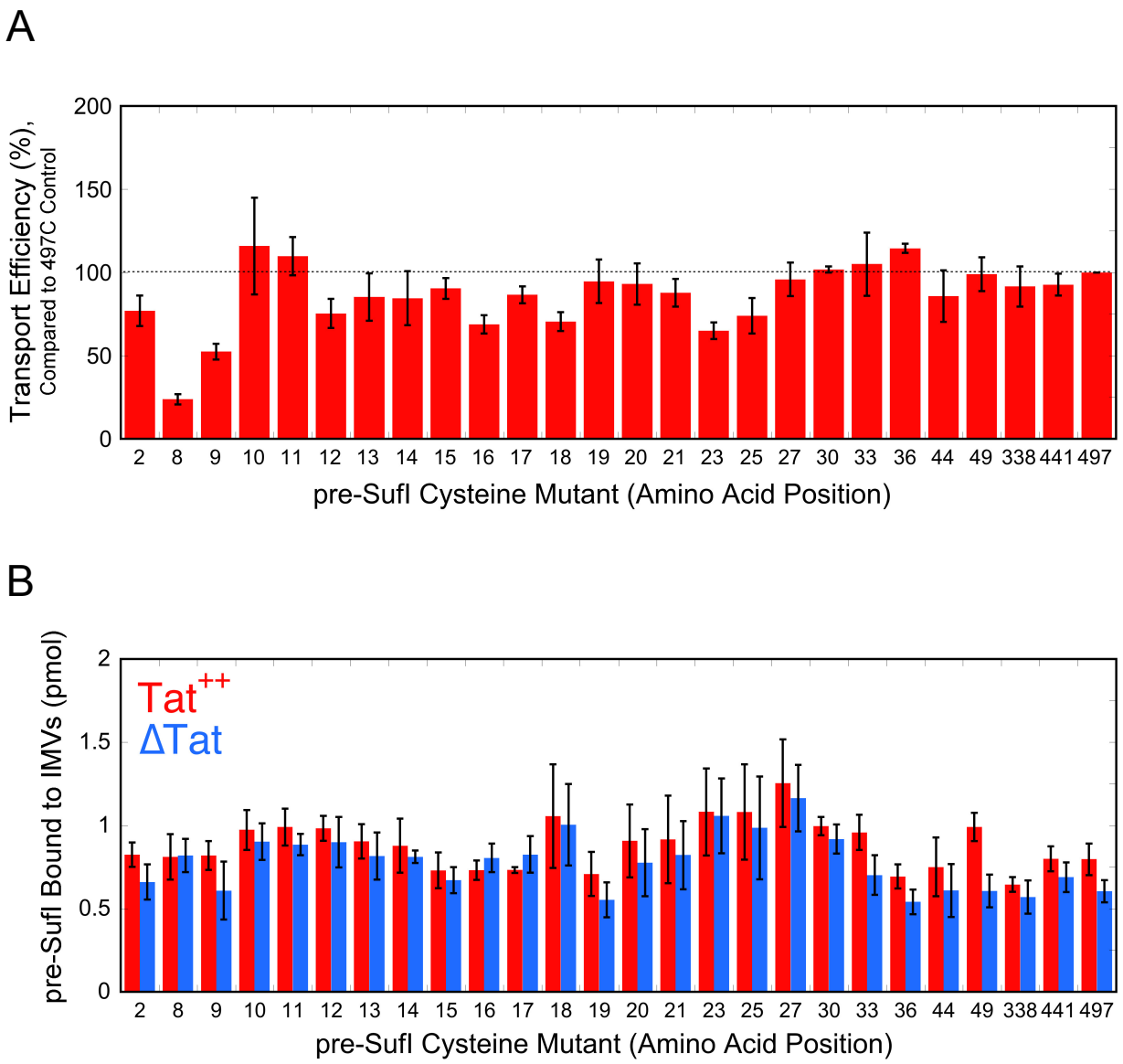

Figure S3. Transport Efficiencies and Membrane Binding of pre-SufI Mutants
(A) *In vitro* Tat Transport Efficiencies for BODIPY-labeled Single Cysteine pre-SufI Mutants. Transport assays were performed by incubating BODIPY-labeled pre-SufI (90 nM) with Tat^{++} inverted membrane vesicles (from *E. coli* strain MC4100 overproducing TatABC; A_{280} = 5). A pmf was generated by addition of NADH (4 mM), and samples were incubated at 37°C for 30 minutes. Untransported protein was digested with proteinase K (0.73 mg/mL for 40 min). Samples were then analyzed by SDS-PAGE, and immunoblotted with SufI antibodies. Most mutants yielded transport efficiencies of ~80-120%, indicating little effect of the mutation and/or dye label. Notable exceptions are the F8C and I9C mutants, which had transport efficiencies of ~20% and ~50%, respectively, likely because of these residues' proximity to the RR-motif.
(B) Membrane Binding of pre-SufI Single Cysteine Mutants. Membrane binding was performed by incubating BODIPY-labeled pre-SufI mutants (90 nM; 3.2 pmol) with ΔTat or Tat^{++} IMVs (A_{280} = 2) at 37°C for 10 min. IMVs were sedimented (16,200 x *g* for 30 min), and analyzed by SDS-PAGE and immunoblotting with anti-SufI antibodies using

pre-SufI concentration standards (N = 3). These data indicate that the labeled pre-SufI mutants bind to Tat-deficient and Tat-containing membranes. However, differences in membrane surface composition and properties can lead to different quantities of lipid-bound precursor under the two conditions. Tat-deficient cells are phenotypically different (chainy phenotype) (1) due to cell division defects, suggesting that differences in IMV properties can be expected. More importantly, the IMV concentration assay is based on an absorbance reading (at 280 nm in 2% SDS), which is highly dependent on the total protein concentration and purity of the IMV preparation. Thus, calculation of the translocon-bound fraction from these data is considered unreliable. The α values determined by our fluorescence approach (Figure S3) are not influenced by these issues.

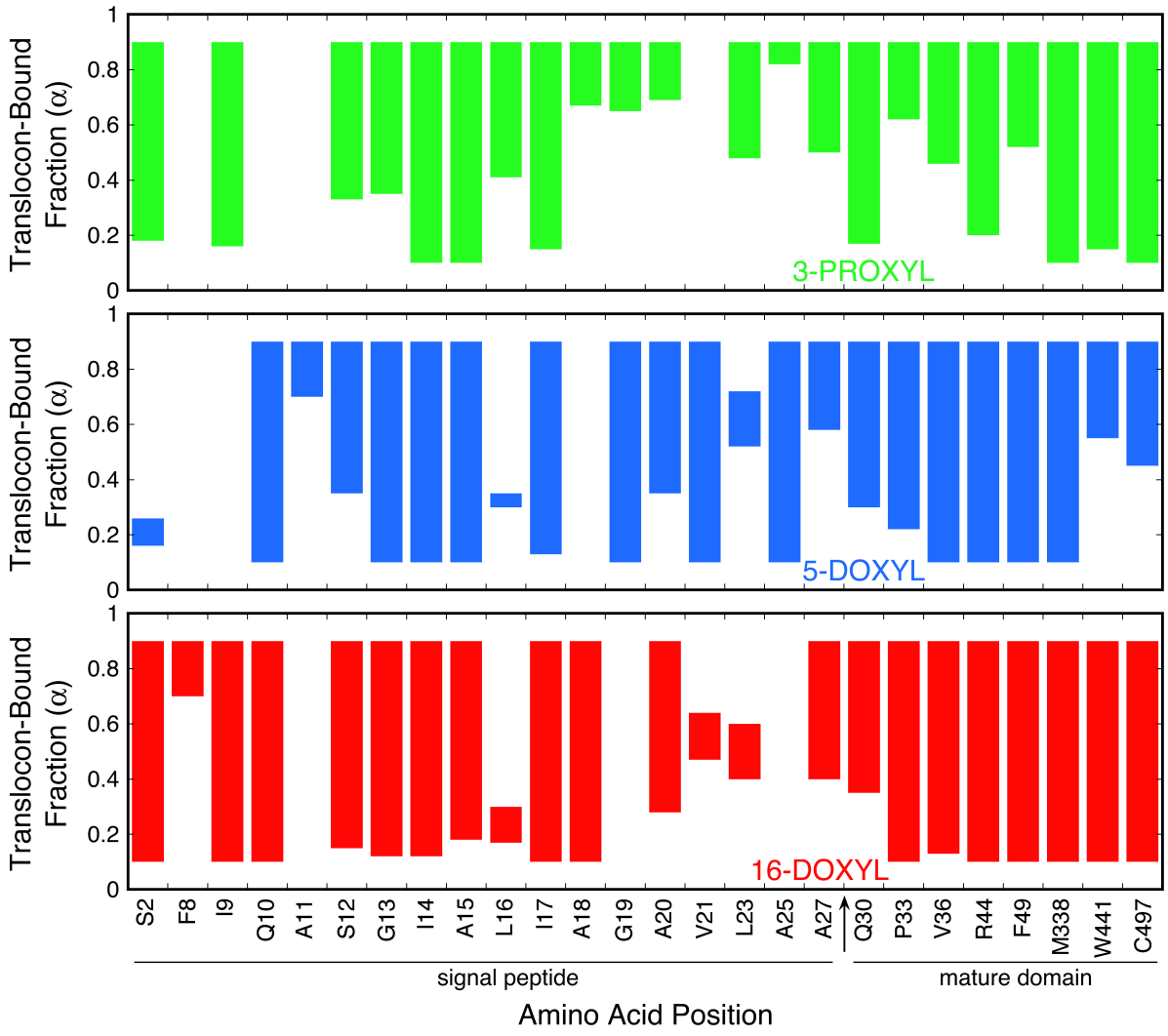

Figure S4. Uncertainty in the α Values for Lipid- and Translocon-Bound pre-SufI. Bars indicate the largest and smallest α values consistent with the fluorescence quenching data (Figures 2 & 3). The translocon-bound fraction (α) was frequently poorly constrained by the data (wide ranges), often because the quenching observed under ΔTat and Tat^{++} conditions was very similar. Comparison of more constrained α values (narrow ranges) reveals that α covered virtually the entire range from 0.1-0.9, suggesting that the various labeled mutants indeed had different lipid and translocon binding affinities. For conditions yielding unreliable K_D values (see Figure 3), α was not determined (blank).

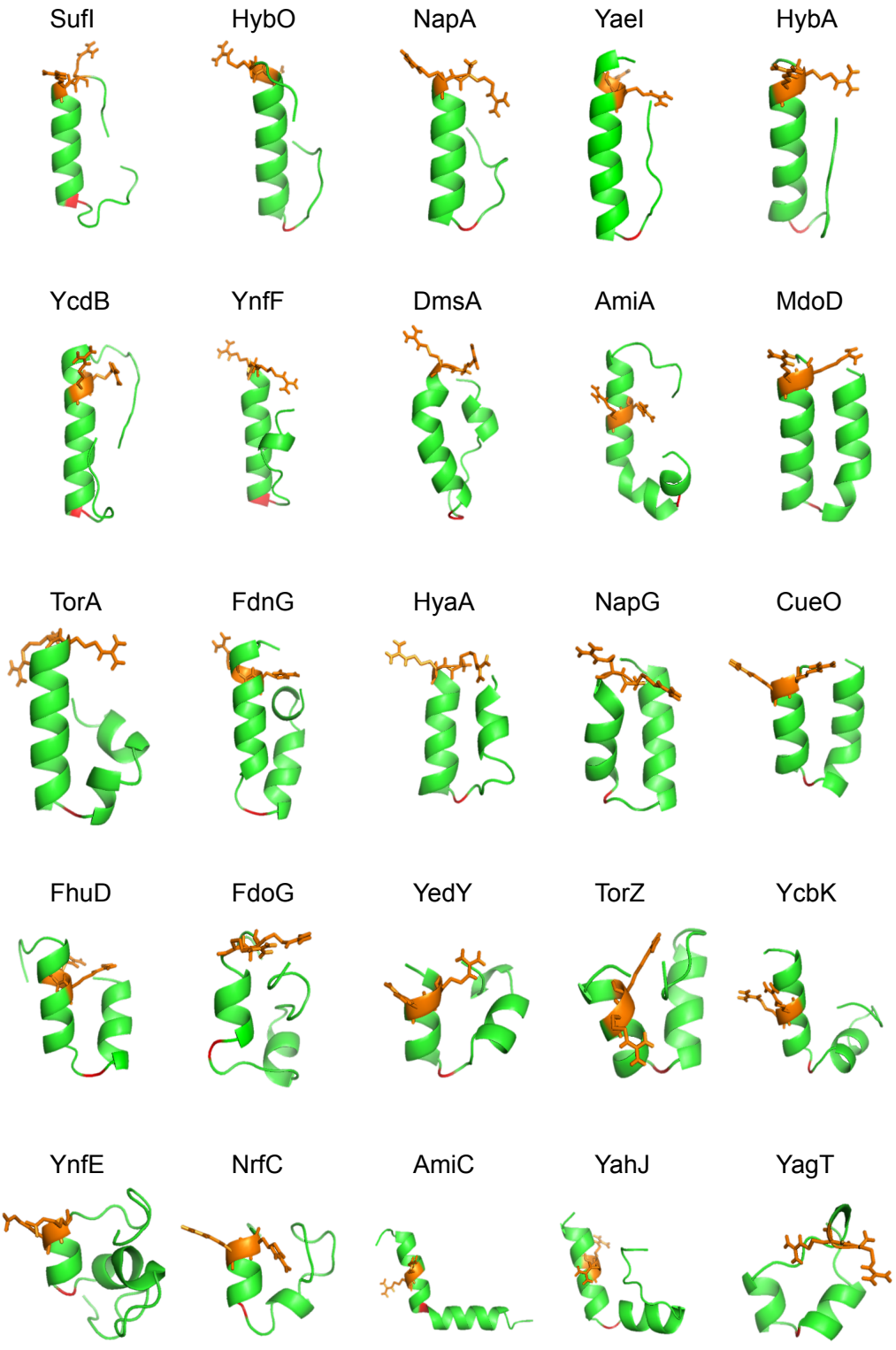

Figure S5. Predicted Secondary Structures of the Signal Peptides from 25 *E. coli* Tat Substrates. Secondary structures were generated as for pre-SufI in Figure 6A. The RR-motif is *orange*. The residue at the end of the first helical region (*red*) is typically glycine (see (B)). The predicted structure for NapA shown here is consistent with its NMR solution structure (PDB ID: 2PQ4).

Figure S6. Signal Peptide Sequences for 25 *E. coli* Tat Substrates. The helix-breaking residues glycine (*green*) and proline (*red*) are identified. The residue(s) after the RR-containing helix as predicted in Figure S5 is circled in *red*, and is (are) typically glycine (20/25, 80%), or occasionally two non-aromatic hydroxyl (S or T) residues (3/25, 12%), which are weak helix-breaking residues (2). The helix destabilizing residue(s) is(are) frequently 12-17 residues after the RR-motif (*blue*), consistent with Figure 6C.

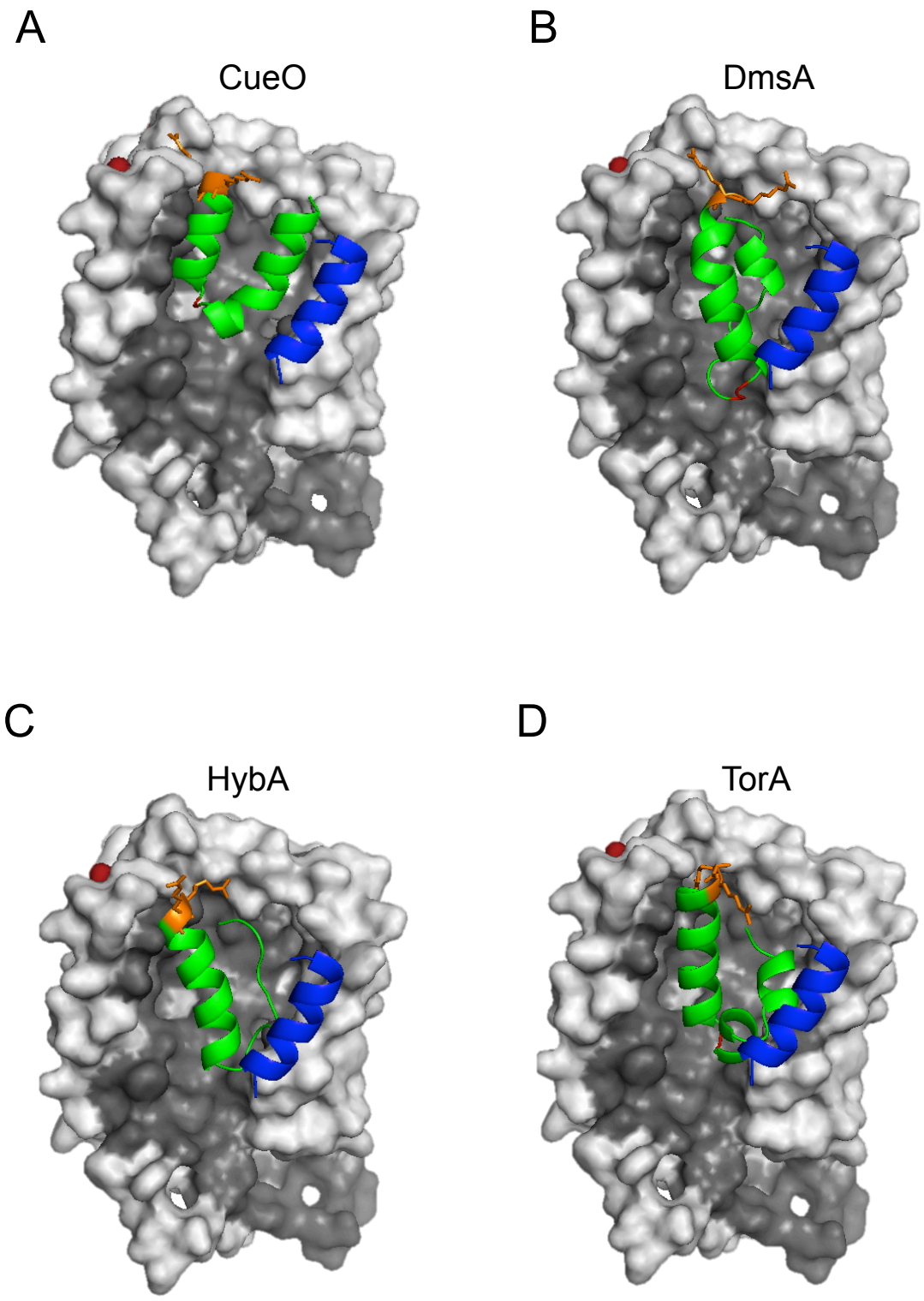

Figure S7. Docked Structures of TatBC with Signal Peptides from Four *E. coli* Tat Substrates. Key: RR-motif (*orange*), helix-destabilizing residue (*red*), TatC (*gray*; SWISS-MODEL ID: P69423), TatB membrane domain (*blue*), glutamic acid residues (E15 and E103 of TatC) involved in binding the RR-motif (*dark red;* more visible in the back view in Figure 6B).

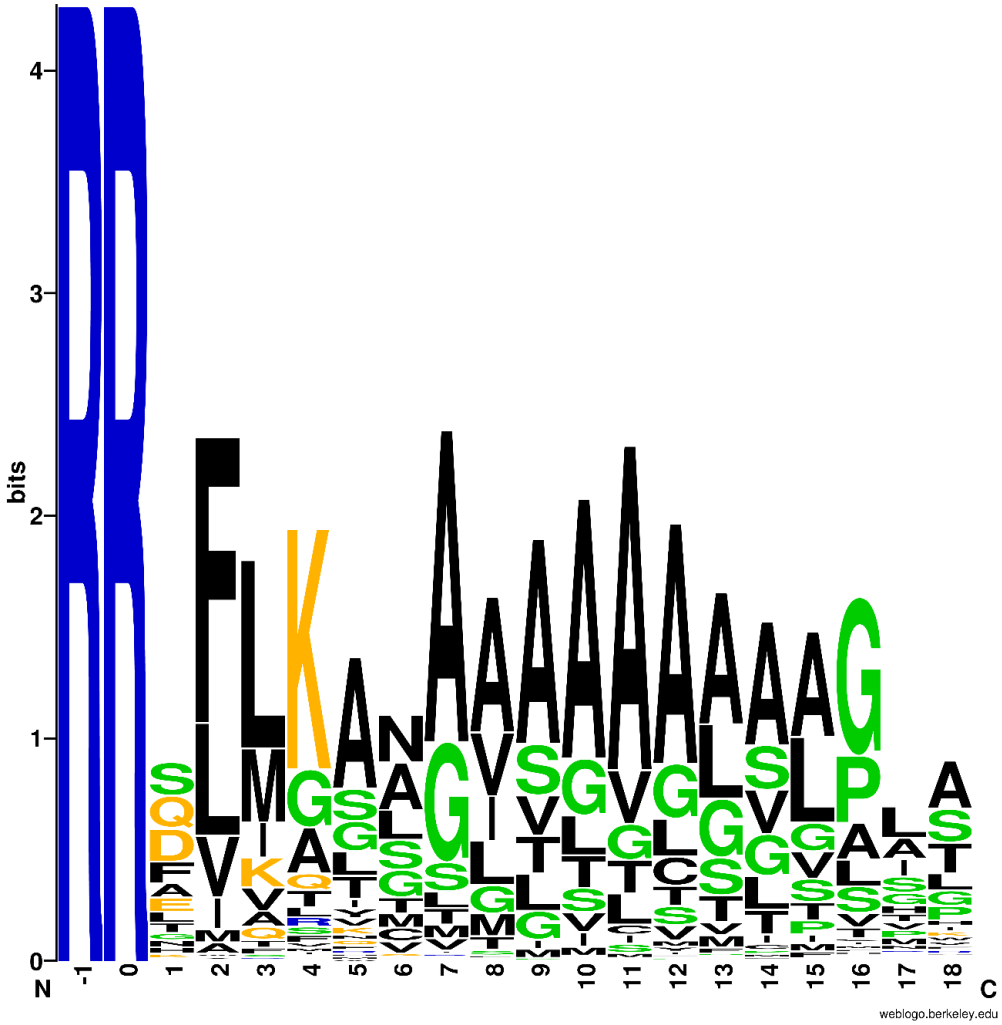

Figure S8. Sequence Logo for the 512 Tat Signal Sequences of Figure 6C. The RRXFLK Tat consensus motif (3, 4) is apparent (-1 to 4), as is the presence of the helix destabilizing residue glycine, which is most predominant 16 residues after the RR-motif. The sequence logo was constructed using web logo tool version 2.8.2 (http://weblogo.berkeley.edu/logo.cgi).

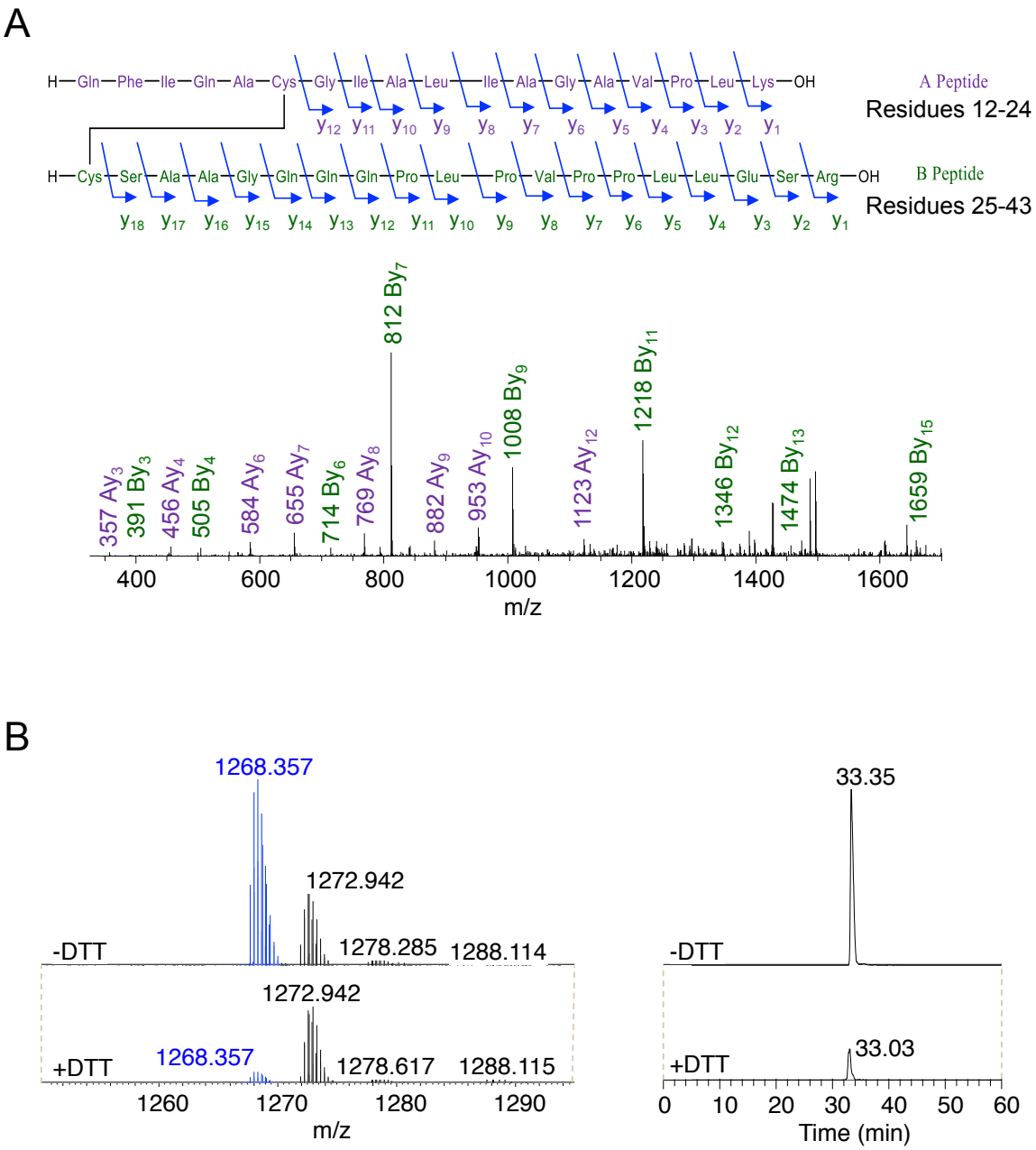

Figure S9. Disulfide Crosslinked pre-SufI(S12C/A25C).
(A) Tandem Mass Spectrometry Analysis of the Disulfide Linked Peptide Fragment of pre-SufI(S12C/A25C). The CID fragmentation spectrum (consisting mainly of +1H adducts) for the peptide ion of m/z = 1268.357 (see Figure 8D). The peak pattern is consistent with a fusion between pre-SufI signal peptide residues 12-24 and 25-43.
(B) Enrichment of the Disulfide-linked Form of pre-SufI(S12C/A25C). The disulfide-linked form of pre-SufI (S12C/A25C) was enriched to ~60% using thiol-reactive SulfoLink Coupling resin (see Materials and Methods). Enrichment was quantified by comparing the ion intensities for peptide B (residues 25-43 of pre-SufI; see (A)) in the presence and absence of DTT, using a closely eluting peak for normalization. The disulfide enriched preparation yielded a substantial increase in the m/z = 1268.357 peak (compare with Figures 8D and 8E).

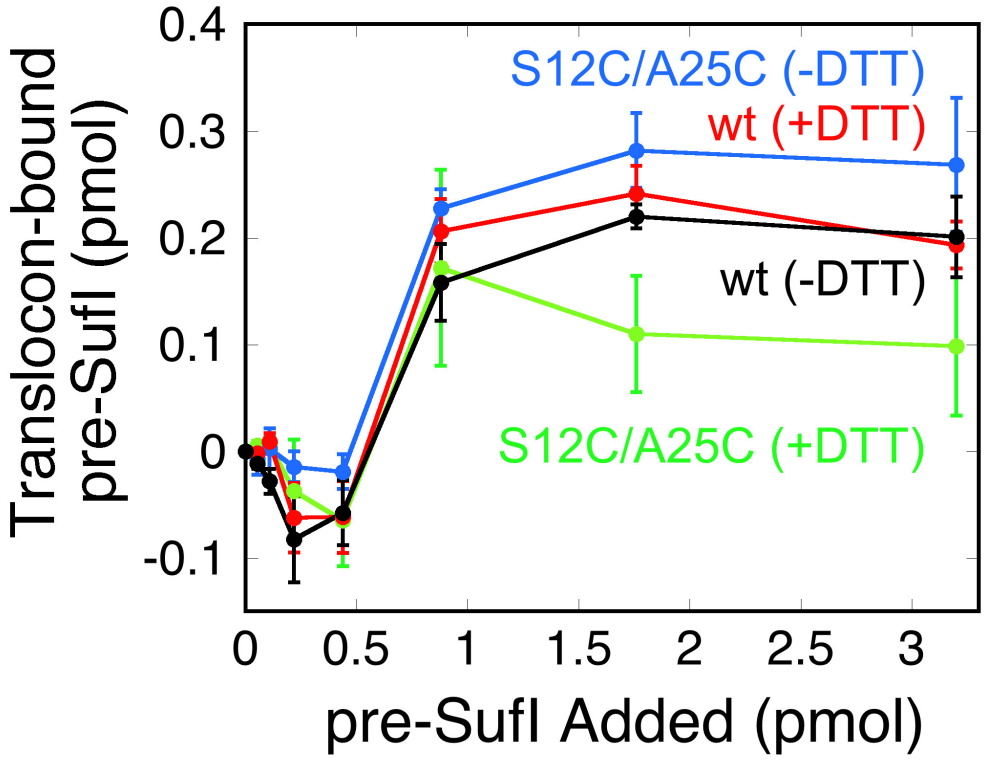

Figure S10. Translocon-bound pre-SufI(S12C/A25C). As described previously (5), the translocon-bound precursor protein is dissociated upon incubation with 2 M urea. Thus, the translocon-bound precursor protein was quantified by subtracting the amount of membrane-bound pre-SufI in 2 M urea (lipid-bound precursor; not shown) from the total membrane-bound pre-SufI (lipid- & translocon-bound precursor; Figure 8G).

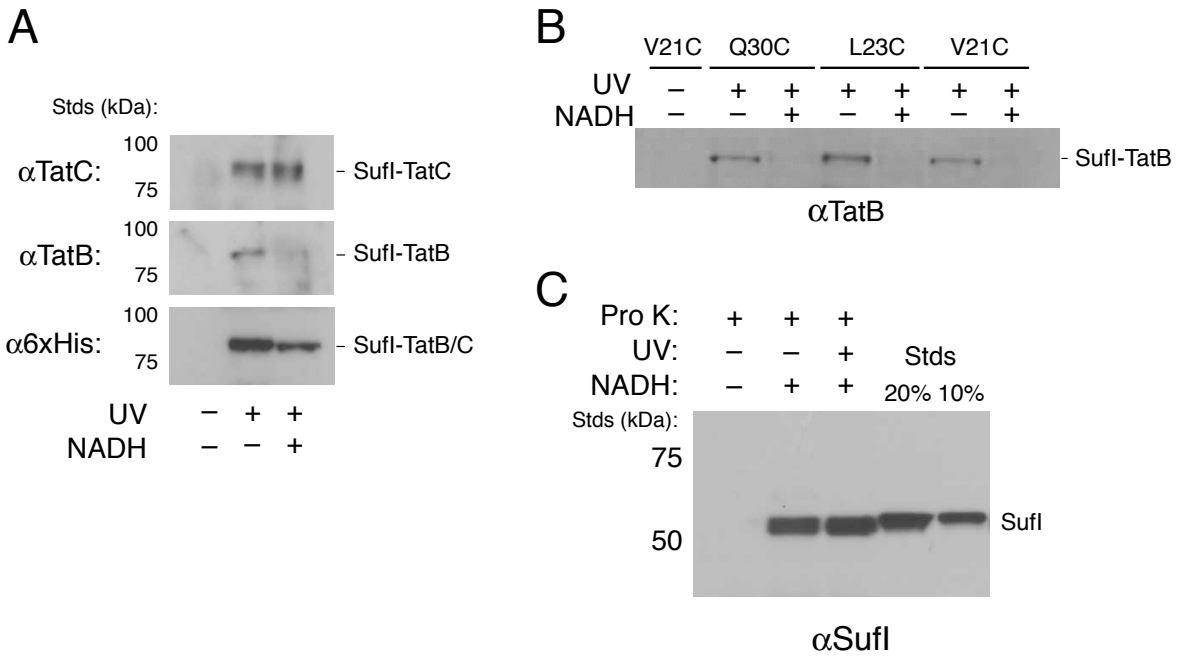

Figure S11. Transportability of Crosslinked Precursor Proteins. (A) Translocation of pre-SufI(V21C) was blocked when crosslinked to TatC. After pre-SufI(V21C) was photocrosslinked to TatC or TatB (as in Figure 7A), the IMV membranes were energized (4 mM NADH for 30 minutes at 37°C). IMVs were recovered by centrifugation (16,200 x *g*, 30 min), and samples were resolved via SDS-PAGE and analyzed via immunoblotting, as indicated. The pre-SufI/TatC adduct remained after membrane energization by NADH, indicating that transport of pre-SufI crosslinked to TatC does not occur (*top*; *N* = 3). In contrast, the amount of pre-SufI/TatB adduct was substantially reduced after membrane energization by NADH, suggesting transport of SufI (*middle*; *N* = 3). The anti-6xHis immunoblot, which detects SufI-6xHis, indicates that the SufI crosslinked to TatB and TatC was reduced by almost half (59±3% remaining) after membrane energization with NADH (*bottom*; *N* = 6). The pre-SufI/TatC and pre-SufI/TatB adducts migrate similarly and hence the bands overlap. The reduction in intensity of the SufI-TatB/C band in the presence of NADH likely results from transport of the pre-SufI/TatB adduct. (B) Translocation of additional pre-SufI mutants crosslinked to TatB. The experiment in (A) was repeated with the V21C, L23C and Q30C mutants of pre-SufI. The amount of crosslinked pre-SufI/TatB adduct was substantially reduced in the presence of NADH, indicating proteolysis, probably by digestion of the adduct after translocation. (C) Transport was not affected by UV illumination. The Tat transport assay was described in Figure 2 – in short, the SufI band observed in the presence of NADH (4 mM) and proteinase K (Pro K, 0.73 mg/mL) represents the transported protein. The pre-SufI concentration standards (Stds) are a loading control in terms of percent precursor added to the reaction mixture, and indicate that ~20% of the initial precursor protein was transported.

The hairpin-hinge hypothesis (Figure 8) predicts that mature domain translocation should not occur when the C-terminal part of the signal peptide is crosslinked to the Tat translocon. The experiments in this figure tested whether signal peptide mutants crosslinked to TatB or TatC could be translocated. We assumed that transport of

crosslinked precursor protein would result in cleavage by signal peptidase, which would be observed as the disappearance of the high molecular weight crosslinked band when membranes were energized with NADH, i.e., the signal peptide would remain crosslinked to TatB or TatC (and indistinguishable from TatB or TatC alone) and the mature domain would be released. Surprisingly, the results conflicted for the V21C mutant, which crosslinks to both TatC and TatB (Figure 7A). The pre-SufI/TatC crosslinked band was retained under transport conditions (A), indicating no transport, and consistent with the hypothesis that signal peptide residues after the hinge residue (G19) must move during transport. In contrast, the pre-SufI/TatB crosslinked band was substantially diminished (A). This latter result was also observed when the pre-SufI mutants L23C and Q30C were crosslinked to TatB (B). All of these results were observed consistently and repeatedly ($N \geq 3$). The Q30C result is especially surprising since this mutation is after the signal peptide cleavage site (between residues 27 and 28) – signal peptidase catalyzed cleavage was expected to only remove the signal peptide from the crosslinked adduct, which would have produced only a minor gel shift (this was not observed). While puzzling, a possible scenario is that TatB is transported with the mature domain, and protease digestion can occur at multiple sites after translocation, resulting in disappearance of the crosslinked adduct. This interpretation is consistent with the SufI immunoblot of the crosslinked protein – under transport conditions, this band get weaker, but does not disappear (A), which is the expected result if the precursor crosslinked to TatB was transported and digested, and that crosslinked to TatC was not. This picture is consistent with the recent hypothesis that TatB is replaced by TatA during transport (6) – more precisely, if the interaction of TatB with the rest of the translocation machinery is broken (required for TatB to be replaced by TatA), the TatB molecule crosslinked to the precursor protein can be transported across the membrane with the mature domain. We do NOT expect that TatB translocation is a normal step in the transport cycle.

SUPPORTING REFERENCES

1. Stanley, N. R., K. Findlay, B. C. Berks, and T. Palmer. 2001. *Escherichia coli* strains blocked in Tat-dependent protein export exhibit pleiotropic defects in the cell envelope. J Bacteriol 183:139-144.
2. Urban, S., and M. Freeman. 2003. Substrate specificity of rhomboid intramembrane proteases is governed by helix-breaking residues in the substrate transmembrane domain. Mol Cell 11:1425-1434.
3. Berks, B. C. 1996. A common export pathway for proteins binding complex redox cofactors? Mol Microbiol 22:393-404.
4. Sargent, F., E. G. Bogsch, N. R. Stanley, M. Wexler, C. Robinson, B. C. Berks, and T. Palmer. 1998. Overlapping functions of components of a bacterial Sec-independent protein export pathway. EMBO J. 17:3640-3650.
5. Bageshwar, U. K., and S. M. Musser. 2007. Two electrical potential-dependent steps are required for transport by the *Escherichia coli* Tat machinery. J Cell Biol 179:87-99.
6. Alcock, F., P. J. Stansfeld, H. Basit, J. Habersetzer, M. A. Baker, T. Palmer, M. I. Wallace, and B. C. Berks. 2016. Assembling the Tat protein translocase. Elife 5:e20718.